The development of in vitro organotypic 3D vulvar models to study tumor-stroma interaction and drug efficacy

Wu, S.D.; Huisman, B.W.; Rietveld, M.H.; Rissmann, R.; Vermeer, M.H.; Poelgeest, M.I.E. van; Ghalbzouri, A. el

Cellular Oncology
https://doi.org/10.1007/s13402-023-00902-w

RESEARCH

The development of *in vitro* organotypic 3D vulvar models to study tumor-stroma interaction and drug efficacy

Shidi Wu[1] · Bertine W. Huisman[2,3] · Marion H. Rietveld[1] · Robert Rissmann[1,2,4] · Maarten H. Vermeer[1] · Mariette I. E. van Poelgeest[2,3] · Abdoelwaheb El Ghalbzouri[1]

Accepted: 15 November 2023

Abstract

Background Vulvar squamous cell carcinoma (VSCC) is a rare disease with a poor prognosis. To date, there's no proper in vitro modeling system for VSCC to study its pathogenesis or for drug evaluation.

Methods We established healthy vulvar (HV)- and VSCC-like 3D full thickness models (FTMs) to observe the tumor-stroma interaction and their applicability for chemotherapeutic efficacy examination. VSCC-FTMs were developed by seeding VSCC tumor cell lines (A431 and HTB117) onto dermal matrices harboring two NF subtypes namely papillary fibroblasts (PFs) and reticular fibroblasts (RFs), or cancer-associated fibroblasts (CAFs) while HV-FTMs were constructed with primary keratinocytes and fibroblasts isolated from HV tissues.

Results HV-FTMs highly resembled HV tissues in terms of epidermal morphogenesis, basement membrane formation and collagen deposition. When the dermal compartment shifted from PFs to RFs or CAFs in VSCC-FTMs, tumor cells demonstrated more proliferation, EMT induction and stemness. In contrast to PFs, RFs started to lose their phenotype and express robust CAF-markers α-SMA and COL11A1 under tumor cell signaling induction, indicating a favored 'RF-to-CAF' transition in VSCC tumor microenvironment (TME). Additionally, chemotherapeutic treatment with carboplatin and paclitaxel resulted in a significant reduction in tumor-load and invasion in VSCC-FTMs.

Conclusion We successfully developed in vitro 3D vulvar models mimicking both healthy and tumorous conditions which serve as a promising tool for vulvar drug screening programs. Moreover, healthy fibroblasts demonstrate heterogeneity in terms of CAF-activation in VSCC TME which brings insights in the future development of novel CAF-based therapeutic strategies in VSCC.

Keywords Vulvar squamous cell carcinoma · Cancer associated fibroblast · 3D model · Tumor invasion · EMT · Chemotherapeutics

Shidi Wu and Bertine W. Huisman contributed equally to this work, shared first authorship.

✉ Abdoelwaheb El Ghalbzouri
a.ghalbzouri@lumc.nl

Shidi Wu
s.wu@lumc.nl

Bertine W. Huisman
bhuisman@chdr.nl

Marion H. Rietveld
m.h.rietveld@lumc.nl

Robert Rissmann
rrissmann@chdr.nl

Maarten H. Vermeer
m.h.vermeer@lumc.nl

Mariette I. E. van Poelgeest
m.i.e.van_poelgeest@lumc.nl

[1] Department of Dermatology, Leiden University Medical Center, Leiden 2333 ZA, The Netherlands

[2] Center for Human Drug Research, Leiden 2333 CL, The Netherlands

[3] Department of Gynecology, Leiden University Medical Center, Leiden 2333 ZA, The Netherlands

[4] Leiden Academic Center for Drug Research, Leiden University, Leiden 2333 CC, The Netherlands

Published online: 07 December 2023

1 Introduction

Vulvar squamous cell carcinoma (VSCC) is the main subtype of vulvar cancer, covering 90% of all cases [1]. Current treatment consists of surgery with or without (chemo) radiotherapy and is associated with significant and long-term side effects. In more than half of the VSCC patients, treatment interventions in the vulvar area result in disfigurement, sexual dysfunction, and psychological problems which cause a significantly reduced health related quality of life for VSCC patients [2]. Despite current treatment modalities, there are high recurrence rates for VSCC patients of up to 40% and 5-year survival rates of 71% remained stable for the last decade. As the prognosis for women with recurrent disease (advanced, regional or distant) is very poor, knowledge and development of new therapies for VSCC is urgently needed [3].

In recent years, the perspective of cancer as a tumor cell-centered disease is shifted to the consensus of the interconnection and dependency of tumor microenvironment (TME), a complex tumor-supporting system which consists primarily of cancer-associated fibroblasts (CAFs) [4]. The conversion of normal fibroblasts (NFs) to CAFs under tumor signaling is one major source of CAF origin, however, the heterogeneity of NFs during this transition is usually neglected. Two subsets of NFs namely papillary (PFs) and reticular (RFs) fibroblasts showed dissimilar morphology, gene profiles and effects to wound healing [5]. Nevertheless, their contributions to VSCC, and their links to CAFs within the VSCC TME remains poorly understood.

To date, no appropriate nonclinical in vitro models are available that mimic human VSCC for more research into VSCC pathogenesis and management [6, 7]. Most vulvar cancer research and drug screening programs are performed in tumor biopsies or (transgenic) animal models [8, 9]. However, mimicking vulvar cancer in animals remains difficult and only one case-report study described the successful establishment of a vulvar xenograft model in a mouse [10]. In addition, due to fundamental species-species differences the obtained data is often difficult to extrapolate to the human situation. Reconstructed 3D-human skin equivalents (HSEs) might be a solution for the issues faced. HSEs, especially the 3D full-thickness models (FTMs) which contain both a differentiated epidermis and a dermis rich of ECM are in vitro-cultured skin models designed to mimic the characteristics of native human skin as closely as possible. HSEs are tools that can be used to study biological processes in the skin including healthy and disease conditions [11–14]. Moreover, HSEs can serve as a prediction model to determine the penetration profile of drugs across the skin [15].

Here, we reported new established in vitro vulvar models for mechanistic and drug evaluation studies. We confirmed the functional link between the heterogeneity of fibroblast subpopulations and the invasive behavior of VSCC, and tested the applicability of the tumorous vulvar models for drug evaluation of chemotherapeutics including carboplatin and paclitaxel. Our study gave a first response to the call for reliable model systems to better understand pathogenesis and improve treatment strategies for VSCC.

2 Methods

2.1 Cell culture

PFs and RFs were isolated from surplus abdominal skin from healthy female donors (age 30–45 years) as previously described [16]. Healthy vulvar epidermal keratinocytes (HVKCs) and healthy vulvar fibroblasts (HVFs) were isolated from surplus healthy vulvar skin obtained from cosmetic labial resections (Roosevelt clinic, Leiden, the Netherlands). In brief, after overnight incubation with Dispase II, the epidermis was separated from the dermis and then further incubated with 0.05% trypsin to acquire keratinocytes. Then a cocktail of collagenase and Dispase II was used to further isolate fibroblasts from the dermis. CAFs were isolated from CSCC primary tumor biopsies obtained from the department of Dermatology (LUMC, Leiden) using the same protocol of isolating HVFs. All resection materials were completely anonymous, no medical history of these patients was required. All primary cells within five passages were used in this study. Fibroblasts were cultured in F5 medium whereas keratinocytes in K5 medium. Two VSCC cell lines A431 (ECACC, Salisbury, UK) and HTB117 (also known as SW954, from ATCC, Virginia, USA) were cultured in K5 medium. Culture medium formula: F5 medium consists of Dulbecco's modified Eagle's medium (DMEM, Gibco) with 5% fetal bovine serum (FBS, Greiner) and 1% penicillin/streptomycin (P/S) (Invitrogen). K5 medium consists of DMEM and Ham's F12 (Gibco/Invitrogen) at 3:1 ratio, supplemented with 5% fetal bovine serum (Bioclot), 1.1 µM hydrocortisone (Sigma), 1 µM isoproterenol, 0.087 µM insulin (all from Sigma-Aldrich) and 1% P/S (Invitrogen). K0 medium: DMEM/Ham's F12 medium (at a 3:1 ratio) + 1% P/S + 0.55 µM hydrocortisone + 1 µM isoproterenol + 0.087 µM insulin + 10 mM L-serine + 50.6 nM selenious acid + 10 µM L-carnitine (Sigma-Aldrich).

2.2 3D organotypic culture of healthy vulvar tissue and VSCC cells

Full thickness models (FTMs) mimicking healthy vulvar tissue or VSCC were established. For healthy vulvar FTMs (HV-FTMs), dermal matrix containing HVFs at a concentration of 10×10^4 cells/ml were generated at Day 1 and

cultured in F5 for a week. Subsequently, at Day 8 a total of 0.25×10^6 HVEKs were seeded on top. For VSCC-FTMs, dermal matrix populated with PFs, RFs or CAFs were generated and then either 7.5×10^4 A431 or HTB117 cells were seeded onto the matrix. At Day 10, all FTMs were cultured for two days at 37 °C and 7.3% CO_2 under submerged condition in K0 medium supplemented with 1% BSA, 1% FBS, 15 µM Linoleic acid, 7 µM Archidonic acid, 25 µM Palmitic acid, 252 µM Vitamin C and 0.95 µM Vitamin E, followed by 2 weeks of culture at air-liquid interface in K0 medium added with the same supplements as described earlier with doubled Linoleic acid concentration and no FBS from Day 12 onwards. Culture medium was refreshed twice a week till harvest. The formula of K0 medium was described in supplementary materials.

2.3 Histopathology and Immunohistochemistry (IHC) analyses

All FTMs were fixed in 4% formaldehyde for 24 h after they were harvested. Fixed tissue was embedded in paraffin and sectioned into 4 µm sections, followed by hematoxylin & eosin (H&E) staining for histopathological observations. For immunohistochemical analyses, FTM sections were incubated with various primary antibodies and secondary antibodies specified in Supplementary Tables 1 and 2 respectively, followed by labelling with a streptavidin-biotin-peroxidase system (GE Healthcare, Buckinghamshire, UK), according to the manufacturer's instructions. Staining was visualized with 3-amino-9-ethylcarbazole, counterstained with hematoxylin and mounted with Kaiser's glycerin. For immunofluorescence staining, slides were counterstained with DAPI.

2.4 Estimation of proliferation index

The proliferation index was determined by an independent researcher who counted the number of Ki67-positive nuclei in a total number of 100 basal cells (×100%) at three locations per slide for three different FTMs. Data represents mean ± standard deviation (SD).

2.5 Quantification of the relative tumor ingrowth

Using Image J (Java) pictures of the H&E staining were converted to grayscale. The whole FTM can be separated into three areas: (A) tumor epidermis, (B) invaded tumor areas in the dermis and (C) the whole dermal matrix. Within the program, boundaries were manually set for each compartment to calculate the corresponding area. The tumor epidermis and dermis was separated by white dash lines and the invaded tumor areas were encircled by blue lines. The relative tumor ingrowth equals the percentage of invaded tumor compartment area in the dermis in each corresponding FTM (B/A + C %) when compared to the control group. Results were presented as the mean ± SD of six counts from three different donors.

2.6 RNA isolation & q-PCR

Materials and methods were as previously described [17]. Primers were designed and evaluated with the amplification efficiency (determined by a dilution range of cDNA) and specificity (determined by gel electrophoresis). The reference genes were selected based on stability using the Genorm program. Sequences for all primers were listed in Supplementary Table 3.

2.7 2D co-culture of CAF with VSCC cells

Conditioned media (CM) from CAFs were obtained from 24 h serum-starved CAFs. Then the CAF-CM was centrifuged at 2000 rpm for 10 min, filtered through a 0.22 µm filter and preserved at − 80 °C freezer for long-term storage. To co-culture CAF with HTB117 or A431 cells, tumor cells were first seeded in a 96-well plate at a density of 5000 cells/well. Then cells were cultured with either F5 or F5 + CAF-CM (1:1 ratio) containing a range of concentrations of Carboplatin (CRP) or Paclitaxel (PTX) for 48 h (Both chemotherapeutics were obtained from the Pharmacy of LUMC, Leiden, Netherlands). Cell viability was detected using WST-1 kits (Roche Diagnostics, Germany) according to the manufacturer's instruction. In brief, after 1 h incubation with the WST-1 reagent at 37℃ in the dark, the absorbance in each well was measured at a wavelength of 450 nm by a Thermo Scientific Microplate Reader (Thermo Fisher, USA) and the IC50 for each drug on tumor cells co-cultured with or without CAFs was calculated.

2.8 Drug efficacy with chemotherapeutics

The anti-proliferative effect of CRP and PTX was first examined on HTB117 and A431 cells in monolayer culture. HTB117 or A431 cells were seeded at a density of 5000 cells/well in 96-well plates 48 h prior to the exposure to a range of concentrations of CRP at 10, 20, 40, 80, 160, 320 and 640 µg/ml and a gradient of concentrations of PTX at 0.5, 1, 2, 4, 8, 18 and 32 nM. Cell viability was detected after 72 h of exposing to the two chemotherapeutics using the WST-1 kit and the IC50 for each drug was calculated. Then, three concentrations representing Low (L), Medium (M) and High (H) were chosen based on the IC50 data to test on FTMs. PF-, RF- and CAF-FTMs seeded with either HTB117 or A431 were established as previously described and divided into 5 groups: the negative control group, CRP-L (1 µg/ml) group, CRP-M (5 µg/ml) group,

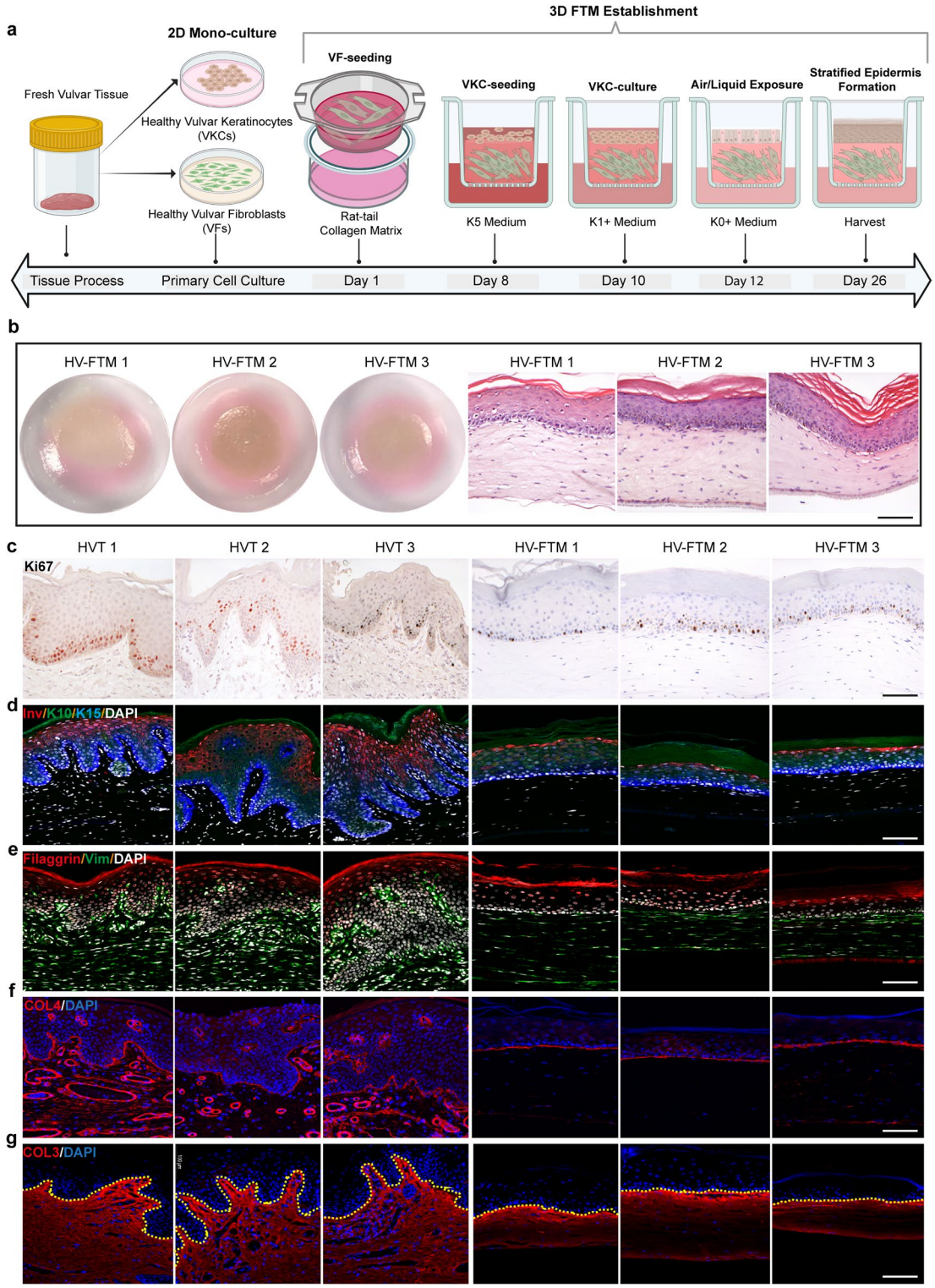

Fig. 1 Comparison between generated HV-FTM and HVT. (**a**) The workflow of establishing HV-FTMs. (**b**) Macro anatomy of HV-FTMs generated from three human donors (left) and their corresponding HE-stained cross sections (right). (**c**) IHC staining of Ki67 on HVT (left) and HV-FTMs (right). (**d**) Triple IF staining of Involucrin (red), K10 (green) and K15 (blue) on HVT (left) and HV-FTMs (right). Cell nuclei were counterstained with DAPI and visualized in white. (**e**) Double IF staining of Filaggrin (red) and Vimentin (green) on HVT (left) and HV-FTMs (right). Cell nuclei were counterstained with DAPI and visualized in white. (**f**) IF staining of COL4 (red) on HVT (left) and HV-FTMs (right). Cell nuclei were counterstained with DAPI and visualized in blue. (**g**) IF staining of COL3 (red) on HVT (left) and HV-FTMs (right). Cell nuclei were counterstained with DAPI and visualized in blue. Yellow dashed lines were drawn to separate epidermis and dermis. Scale bar = 50 μm

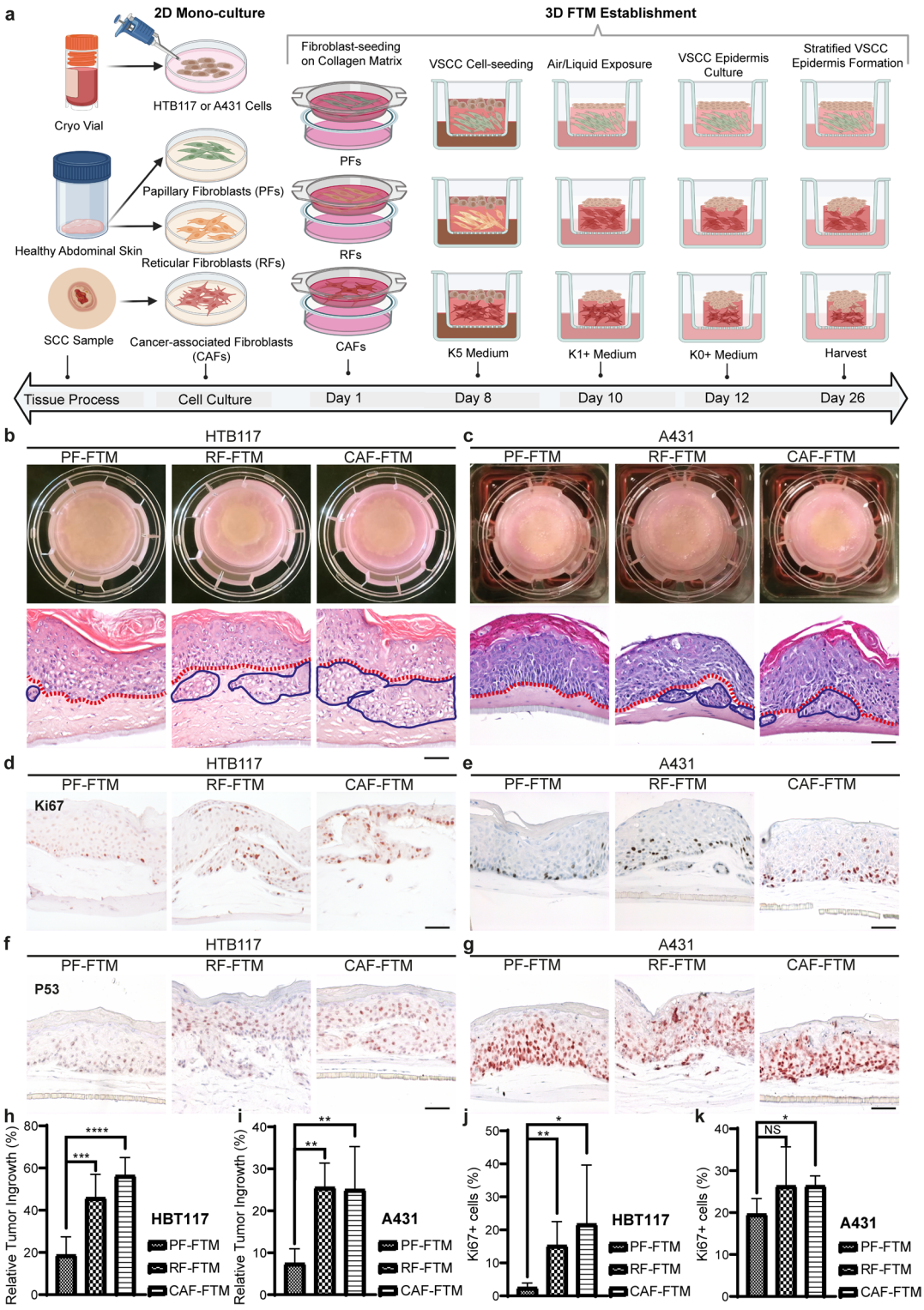

Fig. 2 Generation of A431- and HTB117-FTMs seeded with different fibroblast-populated dermal scaffolds. (**a**) Workflow of the establishment of A431- and HTB117-FTMs populated with PFs, RFs or CAFs. Macro anatomy (top) and HE staining (bottom) of (**b**) HTB117-FTMs based on PF, RF and CAF scaffolds and (**c**) A431-FTMs based on PF, RF and CAF scaffolds. Red dashed lines were drawn to separate epidermis and dermis. Blue lines were used to visualize tumor invasion in the dermal compartment. IHC staining of Ki67 in (**d**) HTB117-FTMs and (**e**) A431-FTMs. IHC staining of P53 in (**f**) HTB117-FTMs and (**g**) A431-FTMs. Statistical analysis was performed on relative tumor ingrowth of (**h**) HTB117- and (**i**) A431-FTMs. Quantification of the positive Ki67 tumor cells in (**j**) HTB117-FTMs and (**k**) A431-FTMs. Data was collected from three independent experiments. Error bars represent ± SD. ** indicates $p < 0.01$, *** indicates $p < 0.001$, **** indicates $p < 0.0001$. Scale bar = 50 µm

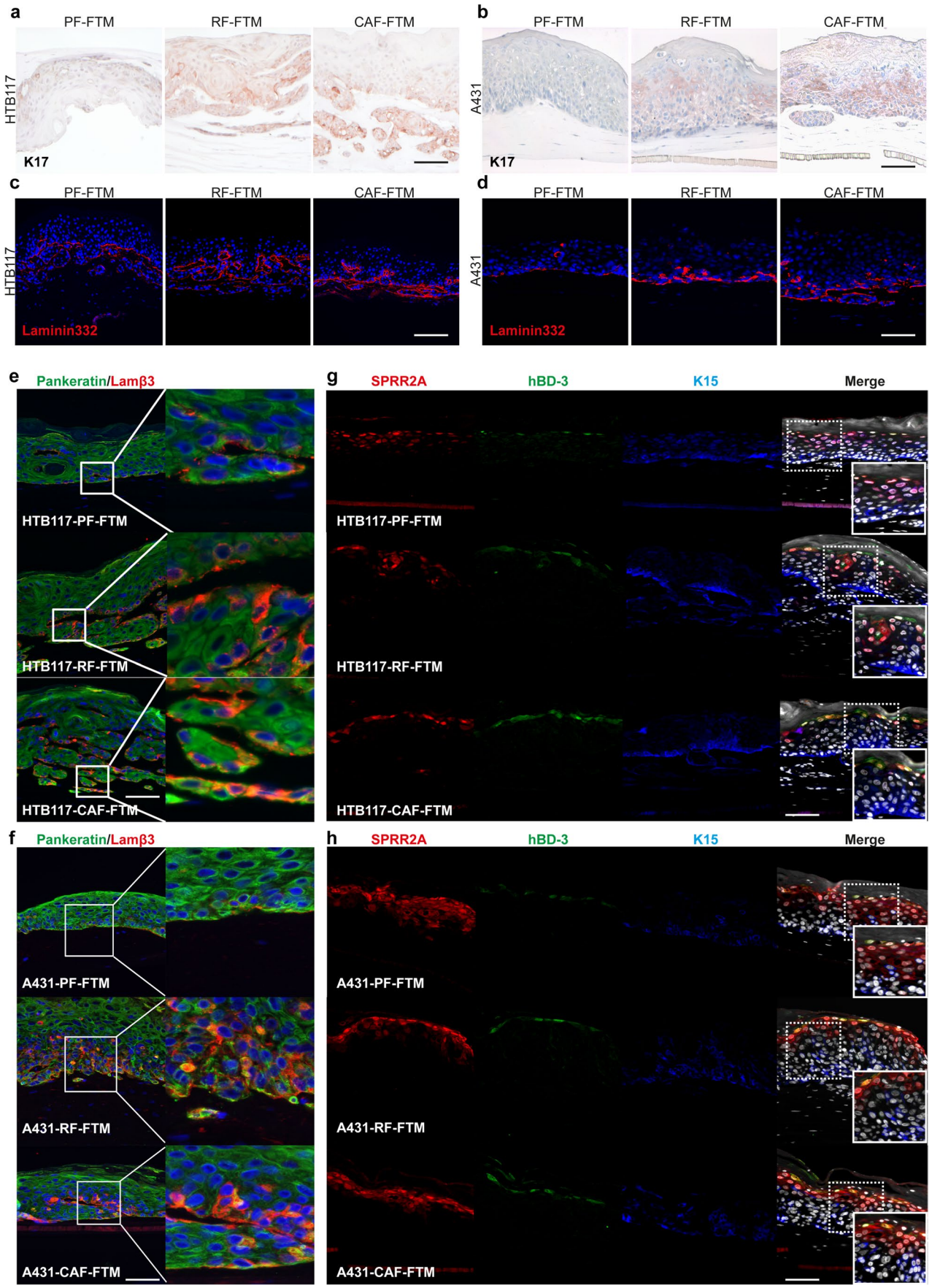
a
PF-FTM
RF-FTM
CAF-FTM
HTB117
K17
b
PF-FTM
RF-FTM
CAF-FTM
A431
K17
c
PF-FTM
RF-FTM
CAF-FTM
HTB117
Laminin332
d
PF-FTM
RF-FTM
CAF-FTM
A431
Laminin332
e
Pankeratin/Lamβ3
HTB117-PF-FTM
HTB117-RF-FTM
HTB117-CAF-FTM
g
SPRR2A
hBD-3
K15
Merge
HTB117-PF-FTM
HTB117-RF-FTM
HTB117-CAF-FTM
f
Pankeratin/Lamβ3
A431-PF-FTM
A431-RF-FTM
A431-CAF-FTM
h
SPRR2A
hBD-3
K15
Merge
A431-PF-FTM
A431-RF-FTM
A431-CAF-FTM

◂**Fig. 3** Tumor morphogenesis of HTB117- and A431-FTMs seeded with different fibroblast subtypes. IHC staining of K17 in (**a**) HTB117-FTMs and (**b**) A431-FTMs. IF staining of Laminin332 (red) in (**c**) HTB117-FTMs and (**d**) A431-FTMs, cell nucleus counterstained with DAPI were visualized in blue. Double IF staining of Pankeratin (green) and Lamβ3 (red) in (**f**) HTB117-FTMs and (**g**) A431-FTMs, cell nucleus counterstained with DAPI were visualized in blue. Triple IF staining of SPRR2A (red), hBD-3 (green) and K15 (blue) in (**g**) HTB117-FTMs and (**h**) A431-FTMs, cell nucleus counterstained with DAPI were visualized in white. Data was collected from three independent experiments. Scale bar = 50 µm

CRP-H (20 µg/ml) group, PTX-L(1nM) group, PTX-M (2nM) and PTX-H (4nM) group. The treatment started at Day 10 and was applied with media refreshment during the 3D culture. After harvest, the FTMs were fixed and embedded for further investigations. Parameters including tumor thickness, tumor cell proliferation, tumor invasion and CAF phenotype were observed.

2.9 Statistic analysis

GraphPad Prism software (version 9.3.1) was used to perform statistical analysis. Dual comparisons were made with an unpaired Student's t-test. One-way analysis of variance (ANOVA) was used for multi-group comparisons. The results of three independent experiments are presented as mean ± SD, and $p < 0.05$ was considered statistically significant.

3 Results

3.1 Establishing 3D healthy vulvar full thickness models (HV-FTMs)

We first established HV-FTMs and investigated to what extent it mimics healthy vulvar tissue (HVT). The whole workflow was demonstrated in Fig. 1a. In brief, dermal matrix populated with HVFs isolated from HVT was cultured for one week, followed by HVKC-seeding on top. Five days later, FTMs were put to air/liquid expose until harvest. Macroscopic pictures and the corresponding HE staining of the HV-FTM from three donors demonstrated a well differentiated epidermis consisting of all epidermal layers and an underlying dermis consisting of evenly distributed fibroblasts in each FTM (Fig. 1b). The epidermal morphogenesis including keratinocyte proliferation (Ki67) (Fig. 1c), early differentiation(Keratin (K) 10) (Fig. 1d), late differentiation (loricrin) (Fig. 1d), basal layer detection (K15) (Fig. 1d), barrier function (Filaggrin) (Fig. 1e) and basal membrane formation (COL4) (Fig. 1f) in HV-FTMs was observed and in accordance with HVT. The distribution of fibroblasts in the HV-FTM-dermis was visualized by Vimentin staining and comparable to the dermis of the human skin (Fig. 1e). COL3 also showed a semblable deposition pattern (Fig. 1g) in HVT-dermis and HV-FTM-dermis. Additionally, the biomarker for cell activation/hyperproliferation K17 was absent in both HVT and HV-FTMs (Supplementary Fig. 1). Above results demonstrated high similarity between HV-FTMs and HVT.

3.2 Distinct effects of PFs, RFs and CAFs on tumor behavior in 3D FTMs generated with VSCC cell lines

In this part, 3D-organotypic cultures mimicking VSCC was performed and the regulation of different fibroblast subtypes on VSCC cell invasion (HTB117 and A431) was explored. The workflow of VSCC-FTM establishment was described in Fig. 2a. First by macroscopic observation, dermis populated with RFs and CAFs showed greater dermal contraction compared to the PFs in both HTB117- and A431-FTMs, indicating a myo-fibroblast trait was gained and preserved in the RF- and CAF-FTMs respectively (Fig. 2b). Morphological analyses revealed a much more profound invasive behavior when the dermal compartment shifted from PFs to RFs or CAFs in both HTB117- and A431-FTMs (Fig. 2b). Further quantification of the tumor ingrowth showed that the area of invaded tumor cell islands (circled by blue line) is more than double in HTB117-RF-FTMs and nearly tripled in HBT117-CAF-FTMs than in HBT117-PF-FTMs (Fig. 2h). In A431-FTMs, the invaded tumor area in RF-FTMs and CAF-FTMs was also significantly increased compared to PF-FTMs (Fig. 2i). In terms of tumor cell proliferation, the fraction of Ki67 positive tumor cells was significantly lower in the HTB117-PF-FTM compared to RF-FTM and CAF-FTM (Fig. 2d). For the A431-FTMs, increased number of Ki67 positive cells were also observed in the RF and CAF group compared to the PF group. However, such difference was less profound than in the HTB117-FTMs. Additionally, P53 was parabasal and diffusely overexpressed in HTB117- and A431-FTMs, yet more pronounced in A431-FTMs (Fig. 2f). HPV-independent status of both cell lines was confirmed by absence of $p16^{INK4A}$ (Supplementary Fig. 2).

3.3 The effect of different fibroblasts subtypes on tumor morphogenesis in 3D VSCC-FTMs

To determine the effect of the fibroblast subtypes on the vulvar carcinoma keratinocytes, specific markers associated with SCC development and progression were analyzed. As shown in Fig. 3a, K17, a marker strongly correlated to SCC aggressiveness was barely expressed in PF-FTMs seeded with both VSCC cell lines, whereas in RF- and

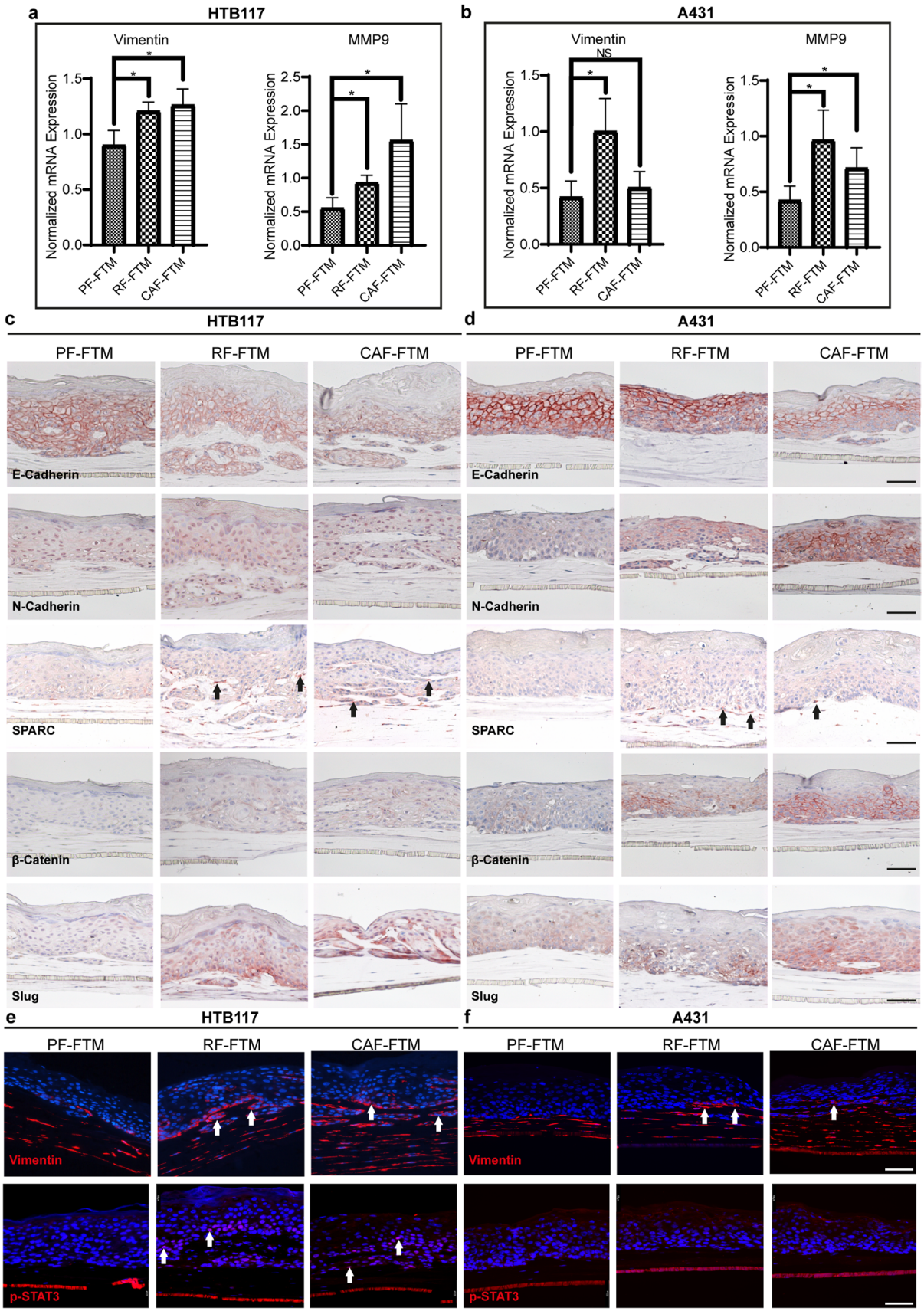
a
HTB117
Vimentin
MMP9
Normalized mRNA Expression
PF-FTM
RF-FTM
CAF-FTM
b
A431
Vimentin
NS
MMP9
c
HTB117
d
A431
E-Cadherin
N-Cadherin
SPARC
β-Catenin
Slug
e
HTB117
f
A431
Vimentin
p-STAT3

◂**Fig. 4** Expression of EMT-related markers in VSCC-FTMs at both mRNA and protein level. The mRNA expression of Vimentin and MMP9 was detected by qPCR in (**a**) HTB117-FTMs and (**b**) A431-FTMs. IHC staining of E-cadherin, N-cadherin, SPARC, β-catenin and Slug in (**c**) HTB117-FTMs and (**d**) A431-FTMs. IF staining of Vimentin (red) and p-STAT3 (red) in (**e**) HTB117-FTMs and (**f**) A431-FTMs. Cell nucleus counterstained with DAPI were visualized in blue. Arrows indicate the positive staining. Scale bar = 50 µm. Data was collected from three independent experiments. Error bars represent ± SD. * indicates $p < 0.05$

CAF-FTMs, elevated expression was observed, especially in CAF-FTMs. Both COL4 (Supplementary Fig. 3a) and Laminin332 (Fig. 3b) staining revealed a more disrupted basement membrane (BM) in RF- and CAF-FTMs compared to PF-FTMs. Moreover, increased expression of Laminin332 was determined in the RF- and CAF-group in both VSCC-FTMs compared to the PF-group. Similarly, the specific β3 chain of laminin family (Lamβ3) which links to the ability of tumor invasion was upregulated in both the RF and CAF group especially on the invasive front compared to the PF group. Dysdifferentiation is universally seen in malignant keratinocytes in SCCs. However, we found out that K10 was diffusely expressed in the suprabasal layers of the epidermis of all FTMs regardless of the corresponding dermal compartments (Supplementary Fig. 3b). In line with this observation, SPRR2A, a precursor of the cornified cell envelope, also showed non-differential expression in all three types of FTMs (Fig. 3g). As for host-defense peptides, hBD-3, an strong effector involved in antimicrobial process which was detected selectively in precancerous and cancerous lesions of SCCs [18], showed enhanced expression in the tumor epidermis when the underlying dermal fibroblast shifted from PFs to RFs or CAFs. To observe the stemness of VSCC keratinocytes, the expression of K19 (Supplementary Fig. 3c) and K15 (Fig. 3g) was detected. An increase of K19 expression was noticed in RF- and CAF-group compared to PF-group in both VSCC-FTMs whereas little difference was shown in K15 expression.

3.4 RFs and CAFs induced tumor cell EMT compared to PFs in 3D VSCC-FTMs

To further explore how different fibroblast subtypes contribute to VSCC invasion, the expression of several EMT-related genes in both VSCC-FTMs was examined. For HTB117-FTMs, an increase of mRNA expression of Vimentin and MMP9 ($*p < 0.05$ for both) was confirmed in the RF-group and CAF-group compared to the PF group. Similarly, MMP9 expression was significantly up-regulated ($*p < 0.05$ for both) in A431-RF-FTMs and A431-CAF-FTMs compared to A431-PF-FTMs whereas enhanced Vimentin expression was only seen in A431-RF-FTMs compared to the corresponding PF-FTMs. The onset of EMT was further validated at protein level by IHC and IF staining in all VSCC-FTMs. For both HTB117 (Fig. 4c) and A431 (Fig. 4d) cell lines, a gradual loss of E-cadherin expression was noticed in the tumor epidermis from PF- to RF- to CAF-group. On the contrary, a gain of expression of several EMT-inducing proteins including N-cadherin, SPARC, β-catenin, and Slug was demonstrated in the RF- and CAF-group compared to the PF-group in A431-FTMs. The majority of up-mentioned factors were also more present in HTB117-RF- and CAF-FTMs compared to the PF ones in which N-cadherin and β-catenin showed little difference. By IF staining, Vimentin was sparsely expressed in PF-FTMs until the dermal component was switched to RFs or CAFs, resulting in positive staining appearing around the invaded tumor area in these FTMs (Fig. 4e and f). Moreover, STAT3 is known to modulate cancer cell EMT, metastasis and stemness [19]. 3D-culturing HTB117 cells with RFs or CAFs induced p-STAT3 expression in the tumor cells, indicating a potential contribution of STAT3 signaling in RF/CAF-mediated tumor cell EMT.

3.5 RFs instead of PFs differentiated into CAFs in 3D VSCC-FTMs

Next, to discriminate the impact of VSCC cells on fibroblast phenotype, all FTMs were stained with two CAF biomarkers (α-SMA and COL11A1), one RF biomarker (TGM2) and one PF biomarker (Decorin). As shown in Fig. 5, when fibroblasts were 3D co-cultured with healthy keratinocytes (control-FTMs), each marker was predominantly expressed in the consistent fibroblast subtype in the dermis. However, a replacement of healthy epidermis by HTB117 or A431 tumor epidermis enabled a robust expression of COL11A1 (Fig. 5a) and α-SMA (Fig. 5b) in RF-FTMs whereas such induction was not observed in the corresponding PF-FTMs. Additionally, a loss of TGM2 expression was observed in RFs co-cultured with HTB117 or A431 cells compared to the control RFs, while Decorin remained considerable expression in the PF-consisting dermis in VSCC-FTMs compared to control PF-FTMs, further suggested that RFs started to differentiate into CAFs (Fig. 5c and d).

3.6 Application of chemotherapeutics for drug evaluation in 3D VSCC-FTMs

To study the potential for anticancer drug efficacy testing of our 3D VSCC models, newly generated HTB117- and A431- -FTMs populated with PFs, RFs or CAFs were treated with Carboplatin (CRP) or paclitaxel (PTX). Before treatment at 3D level, the 72 h IC50 of CRP (Supplementary Fig. 4a) and PTX (Supplementary Fig. 4b) in both HTB117 and A431 cells were determined. Then, CRP and PTX at low (L) medium (M) and high (H) concentrations were

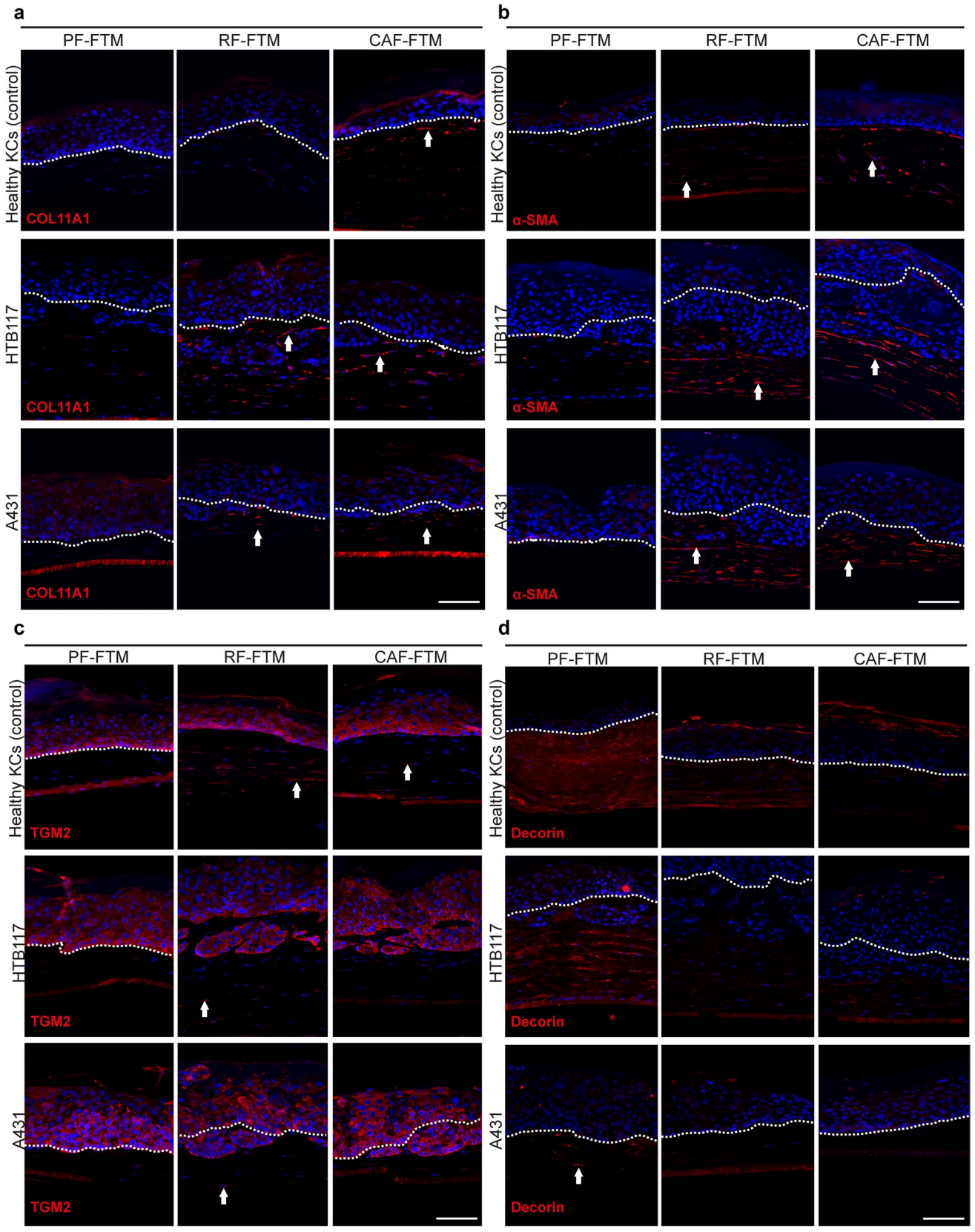

Fig. 5 RF to CAF differentiation in VSCC-FTMs. IF staining of (**a**) COL11A1, (**b**) α-SMA, (**c**) TGM2 and (**d**) Decorin in HTB117- and A431-FTMs. Data was obtained from three independent experiments. Cell nucleus were visualized in blue. Arrows indicate the positive staining. Scale bar = 50 μm

selected based on the IC50 results. As shown in Fig. 6a, application of both chemotherapeutics greatly thinned the tumor epidermis on a dose-dependent manner regardless of the dermal type. Ki67 staining (Supplementary Fig. 5a) showed that the proliferative ability of tumor cells was hugely dampened after treatment with chemotherapeutics in both VSCC-FTMs. Compared to the control groups, much lower amount of residing Ki67 + tumor cells was noticed in the CRP-L and CRP-M groups in HTB117-FTMs whereas corresponding concentrations of CRP showed little effect on A431-FTMs, suggesting distinct sensitivity of these two cell lines to CRP in terms of proliferation. Similarly, the intensity of K17 staining was gradually decreased accompanied by the increase of drug dosage in both VSCC-FTMs (Supplementary Fig. 5b). In PTX-treated FTMs, Low concentration already strongly diminished K17 expression intensity in HTB117 tumor cells in PF-, RF- and CAF-FTMs, whereas A431-FTMs received PTX application with the same concentration remained high K17 expression compared to the corresponding control group. Moreover, 2D co-culturing CAFs with HTB117 and A431 cells led an increase of the IC50 value of both chemotherapeutics in the tumor cells, suggesting important role of CAFs in tumor cell drug-resistance (Supplementary Fig. 6). Despite the decrease in cell number of fibroblasts in the high-concentration treated groups, neither CRP nor PTX treatment attenuated the expression intensity of α-SMA in both VSCC-RF-FTMs and VSCC-CAF-FTMs (Fig. 6b).

4 Discussion

This is the first study that successfully established in vitro healthy human vulvar FTMs with excellent similarities with native healthy vulvar tissue. The presence of four well-differentiated epidermal layers and correct programming of epidermal proliferation and differentiation of native vulvar skin was mirrored in all HV-FTMs, in agreement with dermatologic studies using skin-based FTMs [13, 15]. K15 is primarily expressed in the basal keratinocytes of stratified epithelia and is not compatible with keratinocyte activation [20]. In the contrast, K17 is known to be present in hyperproliferative epithelial cells in chronic wounds and some SCCs, as shown in our RF- and CAF based 3D VSCC models [21, 22]. In our HV-FTMs, K15 was nicely restricted to the basal layer whereas K17 is absent, stipulating the inactivated state of the keratinocytes in these models. Similar deposition of COL4 and COL3 was demonstrated in the basement membrane and dermis respectively when comparing HV-FTMs to HVT, indicating these 3D-cultured fibroblasts mimicked their homologs in real vulvar tissues.

The heterogeneity of NFs were elucidated in VSCC-FTMs. Opposite to PFs, RFs functioned highly similar to CAFs in 3D VSCC models to promote tumor events by inducing the expression of proteins related to disease progression including K17 and several laminins [23–25]. Hyperproliferation of SCC cells is normally associated with poor differentiation. However, neither K10 nor SPPR2A expression showed differential expression in VSCC-FTMs populated with the three fibroblast subtypes, suggesting an universal contribution of fibroblasts on keratinocyte differentiation. We also observed the potential effect of fibroblast subtypes on the stem cell-like properties of VSCC cells, which has been proven to assist therapeutic resistance, tumor dormancy and metastasis [26], by staining all FTMs with K15 and K19. Even though the K15 expression showed no difference between groups, K19 which was reported to be associated with a more aggressive behavior in human skin and hepatocellular tumors [27], was apparently more present in RF- and CAF-FTMs. Additionally, hBD-3 was reported to promote oral SCC cell proliferation and invasion and induces PD-L1 expression in head and neck SCC [28, 29], indicating that this anti-bacterial peptide is also important in SCC pathogenesis. An increase of hBD-3 expression was noticed in RF- and CAF-FTMs compared to PF-FTMs which yielded a potential interesting aspect of fibroblast contribution to VSCC progression.

Hereafter a possibly EMT-like mechanism was evaluated in the fibroblast-mediated tumor progression. The hallmark of EMT in cancer is the downregulation of E-cadherin which and the upregulation of mesenchymal proteins such as vimentin. E-cadherin is repressed by EMT-inducing transcription factors such as TWIST, SNAIL/Slug and ZEB [30, 31]. In line with this, we noticed a decrease of E-cadherin and an overexpression of the majority of EMT-inducing markers included in this study, accompanied by enhanced p-STAT3 expression when the fibroblasts shifted from PFs to RFs and CAFs in the dermis. However, no obvious change in p-STAT3 induction was seen in A431-based FTMs between each fibroblast subtype, potentially due to the distinct reactions of different tumor cell lines to fibroblast interaction. Clearly, more investigations are needed to clarify and validate such observation.

As tumor stroma is an integral part of cancer progression, the communication between fibroblast and epidermal cancer cells was investigated in our models [32]. CAFs expressed a consistent high level of α-SMA and COL11A1 after interaction with VSCC cells, indicating the CAF phenotype was maintained in these FTMs, which might partially explain the profound tumor invasive behavior we observed in CAF-FTMs. Interestingly, after 3D co-cultured with VSCC cells, a loss of TGM2 expression (RF marker) and a gain of striking

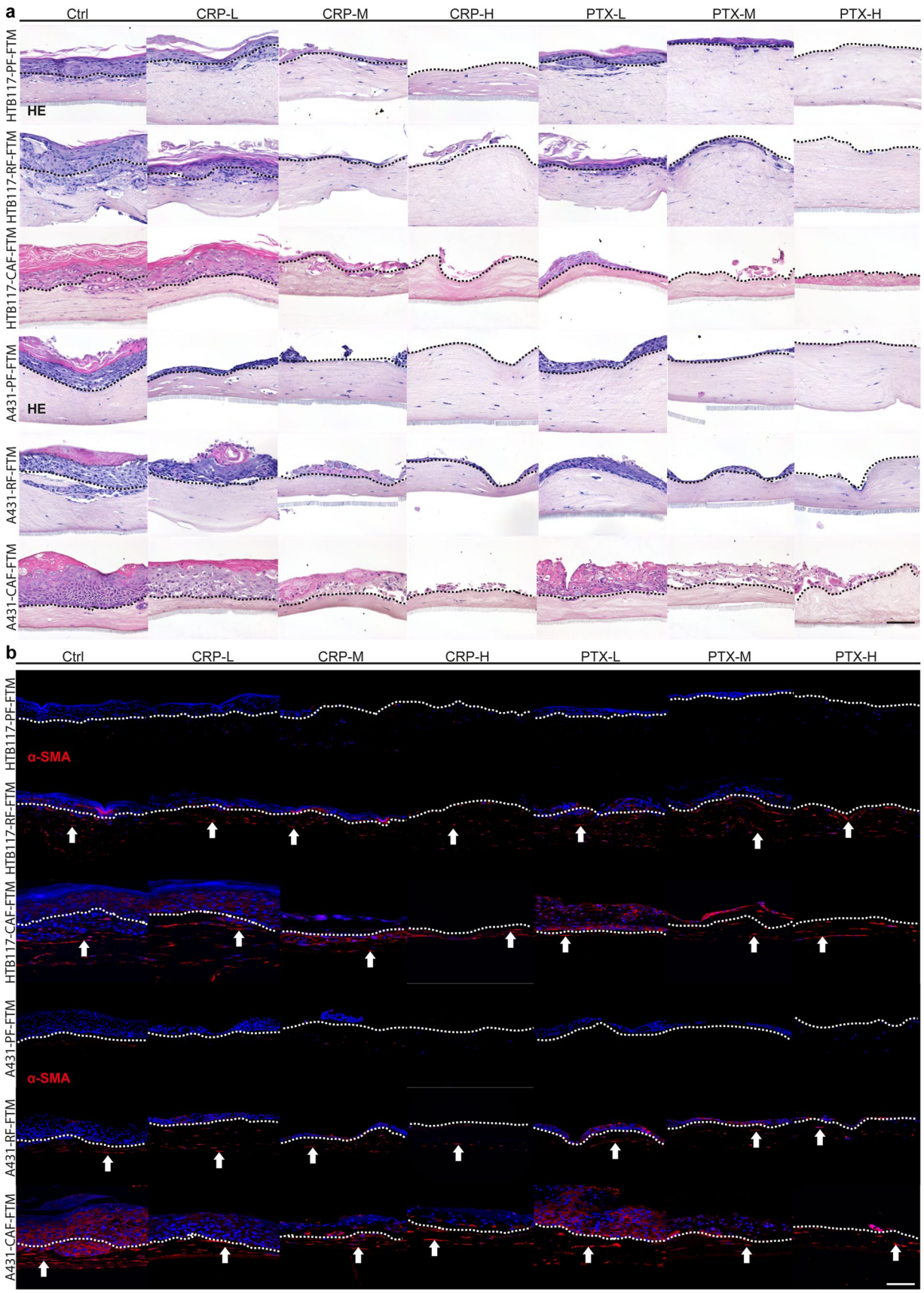
a
Ctrl
CRP-L
CRP-M
CRP-H
PTX-L
PTX-M
PTX-H
HTB117-PF-FTM
HE
HTB117-RF-FTM
HTB117-CAF-FTM
A431-PF-FTM
HE
A431-RF-FTM
A431-CAF-FTM
b
Ctrl
CRP-L
CRP-M
CRP-H
PTX-L
PTX-M
PTX-H
HTB117-PF-FTM
α-SMA
HTB117-RF-FTM
HTB117-CAF-FTM
A431-PF-FTM
α-SMA
A431-RF-FTM
A431-CAF-FTM

◂**Fig. 6** Application and drug evaluation of CRP and PTX on VSCC-FTMs. After treated with or without CRP-L, CRP-M, CRP-H, PTX-L, PTX-M and PTX-H, following assays were performed on HTB117- and A431-FTMs: (**a**) HE staining, black dashed lines were drawn to separate epidermis and dermis, (**b**) IF staining of α-SMA, cell nucleus counterstained with DAPI were visualized in blue, white dashed lines were drawn to separate epidermis and dermis. Data was collected from three different donors. Scale bar = 50 µm

expression of these CAF markers was observed in RF-FTMs, whereas such 'CAF-differentiation' was not observed in PFs interacted with VSCC cells. Although this transition of quiescent fibroblasts appears to be the main progenitor for CAFs [33], the heterogeneity of NFs in CAF acquisition was firstly discussed in this study, therefore bringing insights on more precise CAF-targeting therapy in VSCC.

We preliminarily tested the applicability of the VSCC-FTMs for drug evaluation by applying carboplatin or paclitaxel on 3D VSCC models since these two chemotherapeutics are commonly used for advanced VSCC treatments [34, 35]. Concentrations of each drug were carefully selected according to the IC50 data collected from monolayer cell viability assays and a clear dose-dependent effect of both paclitaxel and carboplatin was observed in the HTB117- and A431-based FTMs, indicating potential use of these 3D VSCC models for future drug screening. Remarkably, chemotherapeutic treatment did not seem to affect the expression intensity of a-SMA in CAFs or RF-shifted CAFs. One of the notorious functions of CAFs is to induce drug resistance. Correspondingly, we noticed higher cell viability of VSCC cells treated with chemotherapeutic when co-cultured with CAFs compared with those without. These observations called attentions for therapeutic interventions on CAFs and its precursor RFs. If these novel models are further qualified and validated, they could offer great potential for research on drug pharmacokinetics [36–38] especially when facing the difficulties recruiting VSCC patients for clinical trials due to the low disease-incidence rates. Moreover, by using the healthy 3D vulvar models, we are able to observe the potential toxicity of the tested drug on healthy tissue [39].

However, some limitations or unexplored aspects of vulvar 3D models should be considered. For instance, skin appendages were currently missing in the HV-FTMs and current research on skin models lacks the immunologic environment as we know is of main importance for VSCCs [32, 40]. Moreover, the models can be improved by introduction of more intratumor heterogeneity and phenotype diversity that the used VSCC cell lines are missing [7]. In the future, 3D vulvar models containing more complex cell components to further characterize healthy vulvar tissue and VSCC would fit in the priorities of our studies.

Overall, we are the first to report an established in vitro vulvar models for VSCC. With our healthy and VSCC-FTMs, we explored the heterogeneity of NFs in 'CAF-activation' process in VSCC TME and proposed a 'RF-CAF' activation process which shed lights in developing new CAF-targeting therapy. Eventually, we gave a first response to the call for reliable model systems to better understand pathogenesis and improve treatment strategies for VSCC.

Supplementary Information The online version contains supplementary material available at https://doi.org/10.1007/s13402-023-00902-w.

Acknowledgements The authors would like to thank the Roosevelt Clinics and the Dermatology department of the LUMC for providing fresh vulvar tissues. The authors thank the donors of the Bontiusstichting (project 8222–32146) of the Leiden University Medical Center for their financial contribution. The authors would also like to thank China Scholarship Council (CSC) for supporting the stay of Shidi Wu in the Netherlands. Graphic abstract, Figs. 1a and 2a were created with BioRender.com.

Author contributions Conceptualization: S.W., B.H, M.P. and A.E.G. Investigation and formal analysis: S.W., B.H and M.R. Writing-original draft preparation: S.W. and B.H. Writing-review and editing: M.P., A.E.G., M.V., and R.R. Supervision: M.P., A.E.G, M.V., and R.R. All authors read and approved the final manuscript.

Funding This study was partially funded by the Bontiusstichting (project 8222–32146).

Data availability The data that support the findings of this study are available from the corresponding author upon reasonable request.

Declarations

Ethics approval Declaration of Helsinki principles were followed during the obtainment of primary cells from human skin originating from surplus breast tissue, vulvar labial tissue and cutaneous tumor biopsies. All subjects remained anonymous. Experiments were conducted in accordance with article 7:467 of the Dutch Law on Medical Treatment Agreement and the Code for Proper Use of Human Tissue of the Dutch Federation of Biomedical Scientific Societies (https://www.federa.org). According to this national legislation, surplus tissue can be used for scientific research purposes when no written objection is made by the informed donor. Therefore, additional approval of an ethics committee regarding the scientific use of surplus tissue was not obligatory.

Consent for publication For the manuscript solitary tissue of anonymous donors was used, no individual person's data was included.

Competing interests The authors declare no competing interests.

References

1. A. Tan, A.K. Bieber, J.A. Stein, M.K. Pomeranz, J. Am. Acad. Dermatol. **81**, 1387–1396 (2019). https://doi.org/10.1016/j.jaad.2019.07.055
2. K.N. Gaarenstroom, G.G. Kenter, J.B. Trimbos, I. Agous, F. Amant, A.A. Peters, I. Vergote, Int. J. Gynecol. Cancer **13**, 522–527 (2003). https://doi.org/10.1046/j.1525-1438.2003.13304.x

3. L.S. Nooij, F.A. Brand, K.N. Gaarenstroom, C.L. Creutzberg, J.A. de Hullu, M.I. van Poelgeest, Crit. Rev. Oncol. Hematol. **106**, 1–13 (2016). https://doi.org/10.1016/j.critrevonc.2016.07.007
4. G. Biffi, D.A. Tuveson, Physiol. Rev. **101**, 147–176 (2021). https://doi.org/10.1152/physrev.00048.2019
5. D.T. Woodley, Dermatol. Clin. **35**, 95–100 (2017). https://doi.org/10.1016/j.det.2016.07.004
6. H. Dongre, N. Rana, S. Fromreide, S. Rajthala, I. Bøe Engelsen, J. Paradis, J.S. Gutkind, O.K. Vintermyr, A.C. Johannessen, L. Bjørge, D.E. Costea, Exp. Cell. Res. **386**, 111684 (2020). https://doi.org/10.1016/j.yexcr.2019.111684
7. K. Lõhmussaar, M. Boretto, H. Clevers, Trends Cancer **6**, 1031–1043 (2020). https://doi.org/10.1016/j.trecan.2020.07.007
8. N.E. Sharpless, R.A. Depinho, Nat. Rev. Drug Discov. **5**, 741–754 (2006). https://doi.org/10.1038/nrd2110
9. J. Chollet, F. Mermelstein, S.C. Rocamboli, D.R. Friend, Int. J. Pharm. **570**, 118691 (2019). https://doi.org/10.1016/j.ijpharm.2019.118691
10. H.T. Nguyen-Xuan, R. Montero Macias, H. Bonsang-Kitzis, M. Deloménie, C. Ngô, M. Koual, A.S. Bats, M. Hivelin, F. Lécuru, V. Balaya, J. Gynecol. Obstet. Hum. Reprod. **50**, 101768 (2021). https://doi.org/10.1016/j.jogoh.2020.101768
11. S. Commandeur, S.J. Sparks, H.L. Chan, L. Gao, J.J. Out, N.A. Gruis, R. van Doorn, A. El Ghalbzouri, Melanoma Res. **24**, 305–314 (2014). https://doi.org/10.1097/cmr.0000000000000079
12. V. van Drongelen, E.M. Haisma, J.J. Out-Luiting, P.H. Nibbering, A. El Ghalbzouri, Clin. Exp. Allergy **44**, 1515–1524 (2014). https://doi.org/10.1111/cea.12443
13. A. El Ghalbzouri, R. Siamari, R. Willemze, M. Ponec, Toxicol. In Vitro **22**, 1311–1320 (2008). https://doi.org/10.1016/j.tiv.2008.03.012
14. R.S. Raktoe, M.H. Rietveld, J.J. Out-Luiting, M. Kruithof-de Julio, P.P. van Zuijlen, R. van Doorn, A.E. Ghalbzouri, Scars Burn Heal **6**, 2059513120908857 (2020). https://doi.org/10.1177/2059513120908857
15. J.A. Bouwstra, R.W.J. Helder, A.E. Ghalbzouri, Adv. Drug Deliv. Rev. **175**, 113802 (2021). https://doi.org/10.1016/j.addr.2021.05.012
16. D. Janson, G. Saintigny, C. Mahé, A.E. Ghalbzouri, Exp. Dermatol. **22**, 48–53 (2013). https://doi.org/10.1111/exd.12069
17. S. Wu, M. Rietveld, M. Hogervorst, F. de Gruijl, S. van der Burg, M. Vermeer, R. van Doorn, M. Welters, A. El Ghalbzouri, Int. J. Mol. Sci. **23**, 11651 (2022). https://doi.org/10.3390/ijms231911651
18. N. Scola, T. Gambichler, H. Saklaoui, F.G. Bechara, D. Georgas, M. Stücker, R. Gläser, A. Kreuter, Br. J. Dermatol. **167**, 591–597 (2012). https://doi.org/10.1111/j.1365-2133.2012.11110.x
19. M. Sadrkhanloo, M. Entezari, S. Orouei, M. Ghollasi, N. Fathi, S. Rezaei, E.S. Hejazi, A. Kakavand, H. Saebfar, M. Hashemi, M. Goharrizi, S. Salimimoghadam, M. Rashidi, A. Taheriazam, S. Samarghandian, Pharmacol. Res. **182**, 106311 (2022). https://doi.org/10.1016/j.phrs.2022.106311
20. A. Waseem, B. Dogan, N. Tidman, Y. Alam, P. Purkis, S. Jackson, A. Lalli, M. Machesney, I.M. Leigh, J. Invest. Dermatol. **112**, 362–369 (1999). https://doi.org/10.1046/j.1523-1747.1999.00535.x
21. I.M. Freedberg, M. Tomic-Canic, M. Komine, M. Blumenberg, J. Invest. Dermatol. **116**, 633–640 (2001). https://doi.org/10.1046/j.1523-1747.2001.01327.x
22. R. Moll, W.W. Franke, D.L. Schiller, B. Geiger, R. Krepler, Cell **31**, 11–24 (1982). https://doi.org/10.1016/0092-8674(82)90400-7
23. O.H. Kwon, J.L. Park, M. Kim, J.H. Kim, H.C. Lee, H.J. Kim, S.M. Noh, K.S. Song, H.S. Yoo, S.G. Paik, S.Y. Kim, Y.S. Kim, Biochem. Biophys. Res. Commun. **406**, 539–545 (2011). https://doi.org/10.1016/j.bbrc.2011.02.082
24. H. Zhang, Y.Z. Pan, M. Cheung, M. Cao, C. Yu, L. Chen, L. Zhan, Z.W. He, C.Y. Sun, Cell Death Dis. **10**, 230 (2019). https://doi.org/10.1038/s41419-019-1320-z
25. M. Tran, P. Rousselle, P. Nokelainen, S. Tallapragada, N.T. Nguyen, E.F. Fincher, M.P. Marinkovich, Cancer Res. **68**, 2885–2894 (2008). https://doi.org/10.1158/0008-5472.Can-07-6160
26. D. Nassar, C. Blanpain, Annu. Rev. Pathol. **11**, 47–76 (2016). https://doi.org/10.1146/annurev-pathol-012615-044438
27. S. Chen, M. Takahara, M. Kido, S. Takeuchi, H. Uchi, Y. Tu, Y. Moroi, M. Furue, Br. J. Dermatol. **159**, 952–955 (2008). https://doi.org/10.1111/j.1365-2133.2008.08731.x
28. M.P. Gomez Hernandez, A.M. Bates, E.E. Starman, E.A. Lanzel, C. Comnick, X.J. Xie, K.A. Brogden, Antibiot. (Basel). 8 (2019). https://doi.org/10.3390/antibiotics8040161
29. Y. Du, Y. Yang, W. Zhang, C. Yang, P. Xu, Transl. Oncol. **27**, 101582 (2023). https://doi.org/10.1016/j.tranon.2022.101582
30. M. Hogervorst, M. Rietveld, F. de Gruijl, A. El Ghalbzouri, Br. J. Cancer. **118**, 1089–1097 (2018). https://doi.org/10.1038/s41416-018-0024-y
31. J.P. Thiery, Nat. Rev. Cancer **2**, 442–454 (2002). https://doi.org/10.1038/nrc822
32. Z. Abdulrahman, K.E. Kortekaas, P.J. De Vos Van Steenwijk, S.H. Van Der Burg, M.I. Van Poelgeest, Expert Opin. Biol. Ther. **18**, 1223–1233 (2018). https://doi.org/10.1080/14712598.2018.1542426
33. K. Räsänen, A. Vaheri, Exp. Cell Res. **316**, 2713–2722 (2010). https://doi.org/10.1016/j.yexcr.2010.04.032
34. P.O. Witteveen, J. van der Velden, I. Vergote, C. Guerra, C. Scarabeli, C. Coens, G. Demonty, N. Reed, Ann. Oncol. **20**, 1511–1516 (2009). https://doi.org/10.1093/annonc/mdp043
35. S.N. Han, I. Vergote, F. Amant, Int. J. Gynecol. Cancer **22**, 865–868 (2012). https://doi.org/10.1097/IGC.0b013e31824b4058
36. H. Wang, P.C. Brown, E.C.Y. Chow, L. Ewart, S.S. Ferguson, S. Fitzpatrick, B.S. Freedman, G.L. Guo, W. Hedrich, S. Heyward, J. Hickman, N. Isoherranen, A.P. Li, Q. Liu, S.M. Mumenthaler, J. Polli, W.R. Proctor, A. Ribeiro, J.Y. Wang, R.L. Wange, S.M. Huang, Clin. Transl. Sci. **14**, 1659–1680 (2021). https://doi.org/10.1111/cts.13066
37. S. Breslin, L. O'Driscoll, Drug Discov. Today **18**, 240–249 (2013). https://doi.org/10.1016/j.drudis.2012.10.003
38. K. Dame, A.J. Ribeiro, Exp. Biol. Med. (Maywood) **246**, 317–331 (2021). https://doi.org/10.1177/1535370220959598
39. S.N. Ooft, F. Weeber, K.K. Dijkstra, C.M. McLean, S. Kaing, E. van Werkhoven, L. Schipper, L. Hoes, D.J. Vis, J. van de Haar, W. Prevoo, P. Snaebjornsson, D. van der Velden, M. Klein, M. Chalabi, H. Boot, M. van Leerdam, H.J. Bloemendal, L.V. Beerepoot, L. Wessels, E. Cuppen, H. Clevers, E.E. Voest, Sci. Transl. Med. **11**, eaay2574 (2019). https://doi.org/10.1126/scitranslmed.aay2574
40. K.E. Kortekaas, S.J. Santegoets, L. Tas, I. Ehsan, P. Charoentong, H.C. van Doorn, M.I.E. van Poelgeest, D.A.M. Mustafa, S.H. van der Burg, J. Immunother Cancer **9**, e003671 (2021). https://doi.org/10.1136/jitc-2021-003671